Post-Repolarization Block of Cloned Sodium Channels by Saxitoxin: The Contribution of Pore-Region Amino Acids

Jonathan Satin, John W. Kyle, Zheng Fan, Richard Rogart, Harry A. Fozzard, and Jonathan C. Makielski
The Cardiac Electrophysiology Laboratories, The University of Chicago, Chicago, Illinois 60637 USA

ABSTRACT Sodium channels expressed in oocytes exhibited isoform differences in phasic block by saxitoxin (STX). Neuronal channels (rat IIa co-expressed with β1 subunit, Br2a + β1) had slower kinetics of phasic block for pulse trains than cardiac channels (RHI). After the membrane was repolarized from a single brief depolarizing step, a test pulse at increasing intervals showed first a decrease in current (post-repolarization block) then eventual recovery in the presence of STX. This block/unblock process for Br2a + β1 was 10-fold slower than that for RHI. A model accounting for these results predicts a faster toxin dissociation rate and a slower association rate for the cardiac isoform, and it also predicts a shorter dwell time in a putative high STX affinity conformation for the cardiac isoform. The RHI mutation (Cys^{374}→Phe), which was previously shown to be neuronal-like with respect to high affinity tonic toxin block, was also neuronal-like with respect to the kinetics of post-repolarization block, suggesting that this single amino acid is important for conferring isoform-specific transition rates determining post-repolarization block. Because the same mutation determines both sensitivity for tonic STX block and the kinetics of phasic STX block, the mechanisms accounting for tonic block and phasic block share the same toxin binding site. We conclude that the residue at position 374, in the putative pore-forming region, confers isoform-specific channel kinetics that underlie phasic toxin block.

INTRODUCTION

Phasic, or use-dependent, block refers to the extra block that develops in response to single or repetitive membrane depolarizations as opposed to tonic block, which is the block developed with infrequent depolarizations. Phasic block is a well known feature of STX and TTX interaction with the relatively toxin-resistant cardiac Na^+ channels (Baer et al., 1976; Cohen et al., 1981; Inoue and Pappano, 1984; Vassilev et al., 1986; Carmeliet, 1987; Clarkson et al., 1988; Eickhorn et al., 1990), but more recently it has become apparent that the toxin-sensitive neuronal channels also show use dependence (Salgado et al., 1986; Lönnendonker, 1989). The modulated-receptor model proposed for phasic block by local anesthetics (Hille, 1977) can be extended to account for phasic block by STX and TTX. The usual interpretation of the model is that a depolarizing step induces a higher affinity conformation or conformations such as the open state or the inactivated state. STX and TTX block the open state in BTX-modified channels (e.g., Krueger et al., 1983), but such block has not been demonstrated in unmodified channels (e.g., Quandt et al., 1985). For TTX, higher affinity binding does occur to a conformation that results from a prolonged depolarizing potential, presumably the inactivated state (Cohen et al., 1981). Salgado et al. (1986), however, demonstrated in crayfish axons that extra block was also induced by depolarizing steps too brief to inactivate the channel. This extra block did not develop while the membrane was depolarized, but after the membrane was repolarized to negative potentials. This block occurring after the membrane is repolarized we call "post-repolarization block" by analogy to the term "post-repolarization refractoriness" (Delmar and Jalife, 1990). Post-repolarization block has been observed in other toxin-sensitive channels (Lönnendonker, 1989; Patton and Goldin, 1991), and it has also been observed in toxin-resistant cardiac channels (Follmer and Yeh, 1988; Makielski et al., 1993). Post-repolarization block of native cardiac channels by STX, however, was distinguished by a >10-fold faster time-course than that reported for the toxin-sensitive channels.

The α-subunits of Na channels from heart (RHI), adult skeletal muscle (μ1), and brain (Br2a) retain their characteristic guanidinium affinities for tonic toxin block when expressed in the *Xenopus* oocyte (Cribbs et al., 1990, Noda et al., 1989, Trimmer et al., 1989). The binding site for guanidinium toxin has been identified as part of the putative pore region (Noda et al., 1989). We have reported recently that mutating the Cys at position 374 in RHI to either a Phe (neuronal-specific) or Tyr (adult skeletal muscle-specific) results in a channel with a high STX sensitivity for tonic block more like neuronal or skeletal muscle channels than heart (Satin et al., 1992a). The reciprocal mutation in the Br2a channel (Phe→Cys) or the μ1 channel (Tyr→Cys) resulted in a Br2a, or μ1 mutant with toxin resistance (Heinemann et al., 1992b; Backx et al., 1992). In regard to phasic block, we noted that the toxin-sensitive pore-region mutants of the cardiac channel developed STX block in response to pulse trains slower than the toxin-resistant wild-type (Satin et al., 1992a). In general, phasic block is less well studied for STX and TTX than tonic block. The exact relationship between the mechanisms for tonic block and phasic

Received for publication 23 July 1993 and in final form 25 February 1994.
Address reprint requests to Jonathan Satin, Medical Center, MC-6094, University of Chicago, 5841 S. Maryland Ave., Chicago, IL 60637. Tel.: 312-702-4447; Fax: 312-702-6789; E-Mail: satin@hearts.bsd.uchicago.edu.

0006-3495/94/05/1353/11 $2.00

block are unknown even for local anesthetics, and the possibility of separate binding sites must be considered (Butterworth and Strichartz, 1990).

In this study, we compare phasic block of cardiac and neuronal isoforms, and demonstrate that the Cys^{374} (Phe in Br2a) residue is responsible for the isoform specific post-repolarization block kinetics. A previously published model for post-repolarization phasic block of cardiac myocytes (Makielski et al., 1993) is used to propose a mechanism underlying the isoform specific post-repolarization block kinetics. This model incorporates the association and dissociation rates of toxin, and rates for the channel transition to a transient, high affinity closed state. A simple difference in the association and dissociation rates of toxin was not by itself sufficient to explain the isoform-specific phasic block kinetics. We must also consider the time the channel dwells in a higher affinity closed conformation. The neuronal and the neuronal-like cardiac mutant require a slower transition from this higher affinity closed conformation than cardiac channels, and consequently a longer dwell time. We conclude that the amino acid at position 374 (Cys in RH1, Phe in Br2a) in the putative pore-forming region plays a role in determining channel kinetics in addition to its importance for toxin affinity. Because mutations at this site also account for isoform differences in tonic block sensitivity (Satin et al., 1992a), our results provide evidence that tonic block and phasic block result from binding at the same site on the channel. Some of these data have been reported in abstract form (Satin et al., 1992c).

MATERIALS AND METHODS

The preparation of cRNA and *Xenopus* oocytes was described previously (Satin et al., 1992b). Point mutations were constructed by creating a polymerase chain reaction (PCR) fragment that encompassed the pore-forming region of repeat I of RHI (Satin et al., 1992a). The PCR product encompassing nucleotides (nt) 197 to 1162 was ligated into a subclone of RHI (pRHI-71) that spanned from nt 445 to nt 2971. From this subclone the *Nsi*I (nt 553) to *Bam*HI (nt 2956) segment was isolated and ligated into an expression vector (pXO1, Satin et al., 1992a). T7 RNA polymerase was used to transcribe the linearized cDNA template.

The rat brain $\beta 1$ subunit was cloned from a rat brain cDNA library using PCR. A 28 base forward primer was synthesized corresponding to bp 201–228 (Isom et al., 1992; 5′-cccaccgccttgcgcggccatggggacg-3′). A 30 base reverse primer was synthesized complementary to bp 867–896 (5′-ggcggagcccagagccagcgctattcagcc-3′). These primers generated a PCR product that contained the entire $\beta 1$ coding sequence including 20 bp upstream of the initiation ATG and 20 bp downstream from the termination TAG. PCR reagents were obtained from Perkin-Elmer (Norwalk, CT), and the PCR reactions were run in a final volume of 100 μl. PCR reactions contained: 1 μg of each primer; 10 mM Tris-HCl, pH 8.3; 50 mM KCl; 1.5 mM $MgSO_4$, 200 μM each dNTP; 1 ng of rat brain cDNA template; and 2 Units of Taq DNA polymerase (Perkin-Elmer). The first cycle of amplification was performed as follows: 94°C for 5 min, 55°C for 90 s, and 72°C for 2 min. The next 30 cycles were performed as follows: 94°C for 1 min, 55°C for 90 s, 72°C for 2 min. The last cycle was followed by a 10-min extension at 72°C. The major PCR product was a band of approximately 740 bp. This fragment was subcloned into pCRII (Invitrogene) and sequenced. The DNA sequence exactly corresponded to that reported by Isom et al. (1992). The $\beta 1$-pCRII plasmid was linearized with *Bam*HI and used as a template for transcription of cRNA as previously described (Satin et al., 1992)

Electrophysiological recordings

Xenopus oocytes were injected with 50–150 ng of cRNA. Three to ten days after injection sodium current (I_{Na}) was recorded from cRNA-injected oocytes with a two electrode voltage clamp/bath clamp. Either a Dagan CA-1 (bath clamp) or a Dagan TEV-200 with a series resistance compensation circuit (TEV-208, Dagan) was used to make recordings. All recordings were made at 20–22°C in a flowing bath solution consisting of (in mM): 90 NaCl, 2.5 KCl, 1 $CaCl_2$, 1 $MgCl_2$, and 10 HEPES, pH 7.4. The electrodes contained 3 M KCl and had resistances that ranged from 0.2 to 1.5 MΩ. Data were acquired using Axobasic 1.1 software onto an Intel-486-based computer. Data were digitized at 42 kHz and were low pass filtered at 10 kHz (−3 dB). The large membrane area of the oocyte (about 1 mm diameter spheres; Cm > 200 nF) prevents the command potential ($V_{command}$) from rising fast enough after step changes to study activation of Na currents. The peak of the Na current ranged from about 1.5 to 3 ms after the onset of $V_{command}$. We monitored and recorded the transmembrane voltage (V_m) as the potential difference between a third bath electrode and the voltage-sensing electrode impaled in the oocyte. Data were discarded if there was a change in the timecourse of V_m after a $V_{command}$ step during the course of the experiment. At the time of the measurement of peak I_{Na} V_m was within 1 mV of $V_{command}$. The possible errors caused by problems with voltage control must be considered for any study of Na current in oocytes. In this study we assumed that the peak current we measured in the second pulse of a pulse pair was a measure of occupancy in the rested or closed states (Fig. 3). This measure appears to be less dependent upon rapid charging of the membrane. In this regard it is reassuring that the results for RHI in oocytes are very similar to those reported for a voltage clamp in rat ventricular cells (Makielski et al., 1993) where membrane charging times were less than 100 μs. In oocytes the rise time of V_m for a $V_{command}$ from −100 to −15 mV was typically less than 600 μs. We did not capacitance- or leak-correct whole-oocyte currents. Leak correction was unnecessary because the expressed currents in the range studied were greater than 10-fold the amplitude of endogenous oocyte currents (predominantly relatively slow outward currents, c.f., Barish, 1983). We never detected an endogenous oocyte Na current. TTX and STX (Calbiochem, LaJolla, CA) were added to the flowing bath from a concentrated stock solution. The bath volume was generally less than 500 μl. To ensure that a known concentration of toxin was attained 4–5 volumes of solution were changed before recording commenced.

Post-repolarization block three-state model

A function $B(t)$ describing the time course of fractional occupancy in the blocked state (C·B in Fig. 4) is

$$B(t) = [STX]k_{CB}(c_w + c_x)/(\lambda_1 - \lambda_2) + k_{RC}k_{CB}c_y/(\lambda_2 - \lambda_1),$$

where [STX] is the toxin concentration in μM and

$$\lambda_1 = (-k+b)/2$$

$$\lambda_2 = (-k-b)/2$$

and where

$$c_w = (R_0 - B_0(\lambda_2 + k_{BC})/([STX]k_{BC}))\exp(\lambda_1 t)$$

$$c_x = (B_0(\lambda_1 + k_{BC}/([STX]k_{CB}) - R_0)\exp(\lambda_2 t)$$

$$c_y = (1 - \exp(\lambda_1 t)/\lambda_1 - (1 - \exp(\lambda_2 t))/\lambda_2$$

$$k = k_{RC} + k_{CR} + [STX]k_{CB} + k_{BC}$$

$$b = ((k^2) - 4k_{RC}[STX]k_{CB} - 4k_{BC}(k_{RC} + k_{CR}))^{1/2},$$

and where the rate constants account for toxin binding k_{CB} s^{-1} μM^{-1} and unbinding k_{BC} s^{-1}, and for the rates for entering k_{RC} (s^{-1}) and leaving k_{CR} (s^{-1}) the high affinity state of the channel and R_0 and B_0 are the initial fractional occupancies in the R and B states, respectively ($R + B + C = 1$). This equation was derived from the set of three simultaneous differential equations describing the dynamic process (see Makielski et al., 1993 for details).

The fraction of current remaining in the second pulse of the pulse-pair experiments was then assumed to represent the fraction of channels not blocked ($1 - B(t)$) at time t after the first pulse. The solution is not unique and depends upon the initial conditions. We used two different sets of initial values for the data normalized in two different ways. For data normalized to first pulse (the principle way we chose to treat the data), we assumed no initial occupancy in B, that is, we assumed the B state accounted for none of the tonic block. For the fit on the inset of Fig. 5 B we assumed an initial occupancy in state B, the value of which was obtained from the dose-response relationship for first pulse block (Fig. 1). For these fits we normalized the data to control currents (in the absence of STX).

$B(t)$ was fit to the data using the SAS (Cary, NC) NLIN nonlinear least-squares fitting procedure using the Gauss method with a CONVERGE criteria of 0.0001 running on a Sun Sparcstation SLC.

RESULTS

Tonic STX block distinguishes neuronal from cardiac Na channel isoforms

The Brain 2a Na channel α-subunit (Br2a) expressed in oocytes is more sensitive to tonic STX block than the rat heart I (RHI) Na channel α-subunit (Fig. 1). Tonic block is defined as the fraction of current measured in response to the first depolarizing step after at least 60 s at a holding potential of -100 mV for wild-type RHI and at least 150 s for the STX-sensitive channels. A longer time at the holding potential was required for the STX-sensitive channels because, as demonstrated below, they take a longer time to recover from phasic block. We also tested whether or not the β1 subunit altered STX blocking affinity. The tonic-block dose response (Fig. 1) shows that co-expression of β1 with Br2a does not alter tonic block. For Br2a expressed in oocytes, the sodium current (I_{Na}) decay and recovery from inactivation is slower

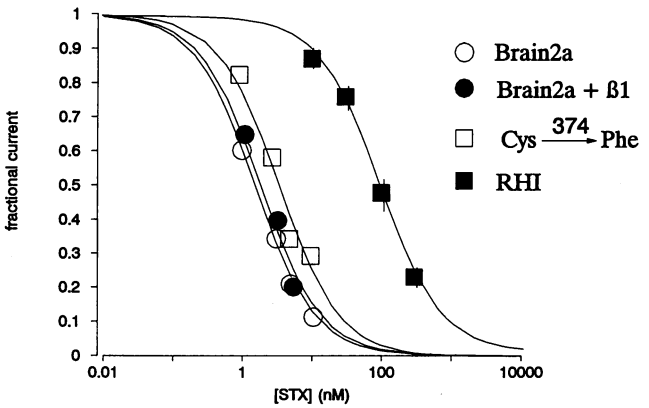

FIGURE 1 Dose response for tonic block of I_{Na} by STX. Tonic block was measured for the Br2a α-subunit alone (○); Br2a + β1 (●), the RHI mutant $Cys^{374}\rightarrow Phe$ (□), and for RHI alone (■). Dose responses were fit to a single-site equation of the form: $(1 + [STX]/k_{1/2})^{-1}$ where $k_{1/2}$ is the STX concentration causing half-block. Co-expression of the β1 subunit with the Br2a α-subunit had no effect on the $k_{1/2}$. Before application of the test pulse the holding potential was maintained at -100 mV for at least 150 s for the STX-sensitive channels (Br2a, Br2a + β1, and $Cys^{374}\rightarrow Phe$) and at least 60 s for RHI to allow full recovery from phasic block. The data are mean values of four to six cells with SD bars shown only when larger than the symbol size. The $k_{1/2}$ values for Br2a (5 cells), Br2a + β1 (4 cells), $Cys^{374}\rightarrow Phe$ (6 cells), and RHI (6 cells) were 1.5, 1.8, 3.5, and 91 nM, respectively.

than I_{Na} in native preparations; however, co-expression of Br2a with the β1 subunit (Br2a + β1) speeds the rate of decay (Isom et al., 1992) and recovery from inactivation of the channel. Because Br2a + β1 retains the tonic block characteristics of Br2a while displaying faster, more native-like kinetics, we studied phasic block of Br2a in the presence of β1. We previously showed that mutating Cys^{374} of RHI to the adult skeletal muscle specific Tyr results in higher STX affinity (Satin et al., 1992a). Fig. 1 shows that the RHI mutant $Cys^{374}\rightarrow Phe$ (Phe being the Br2a-specific residue at RHI equivalent position 374) displays tonic STX block ($k_{1/2} = 3.5$ nM) that is greater than wild-type RHI ($k_{1/2} = 91$ nM) and is similar to that for Br2a + β1 ($k_{1/2} = 1.8$ nM).

Phasic STX block of neuronal channels develops slower than that of cardiac channels

Fig. 2 shows current traces elicited by a train of 7 ms long depolarizing steps from -100 to -10 mV at a frequency of 2 Hz for Br2a + β1 (Fig. 2 A) and for RHI (Fig. 2 B). Currents in the absence of STX are superimposed on currents elicited by the 1st, 10th, and 50th pulses of the 2-Hz train in the presence of an approximate half-tonic blocking concentration of STX. Phasic block by STX is manifested as the progressive decrease in peak current during pulse trains. The rate of phasic block development for RHI ($\tau = 2.6$ pulses, Fig. 2 D) is faster than that for either Br2a + β1 ($\tau = 9.1$ pulses, Fig. 2 C) or the STX-sensitive RHI mutant $Cys^{374}\rightarrow Phe$ ($\tau = 18$–24 pulses, $n = 4$, data not shown). For all channel types tested, the normalized amplitude and rate of development of phasic block was greater for increasing STX concentration. The difference in the rates of development of phasic block, however, cannot be accounted for by differences in toxin concentration alone. When identical STX concentrations were tested, the wild-type RHI developed phasic block faster than the toxin-sensitive Br2a + β1 and $Cys^{374}\rightarrow Phe$, and block was slower for the more toxin-resistant $Arg^{377}\rightarrow Asn$ mutant (data not shown).

Post-repolarization STX block and maintained (inactivated) state block of RHI

A two-pulse protocol was used to assess phasic block and recovery from inactivation. An initial depolarizing step (the conditioning pulse) was used to elicit transitions out of the resting state. A second depolarizing step (test pulse) followed the conditioning pulse after a variable interval at -100 mV to assess the fraction of channels made unavailable by the conditioning pulse. An example of such a protocol is shown in Fig. 3. When the conditioning pulse was brief (10 ms), complete recovery from fast inactivation of wild-type RHI occurred within 100 ms (Fig. 3 A, *open triangles*). In the presence of 100 nM STX, three phases of block are evident (Fig. 3, A and B, *filled triangles*) and can be interpreted as: 1) a fast rising phase representing recovery from inactivation, 2) a falling phase corresponding to the development of phasic STX block, and 3) the final, slowly rising phase representing

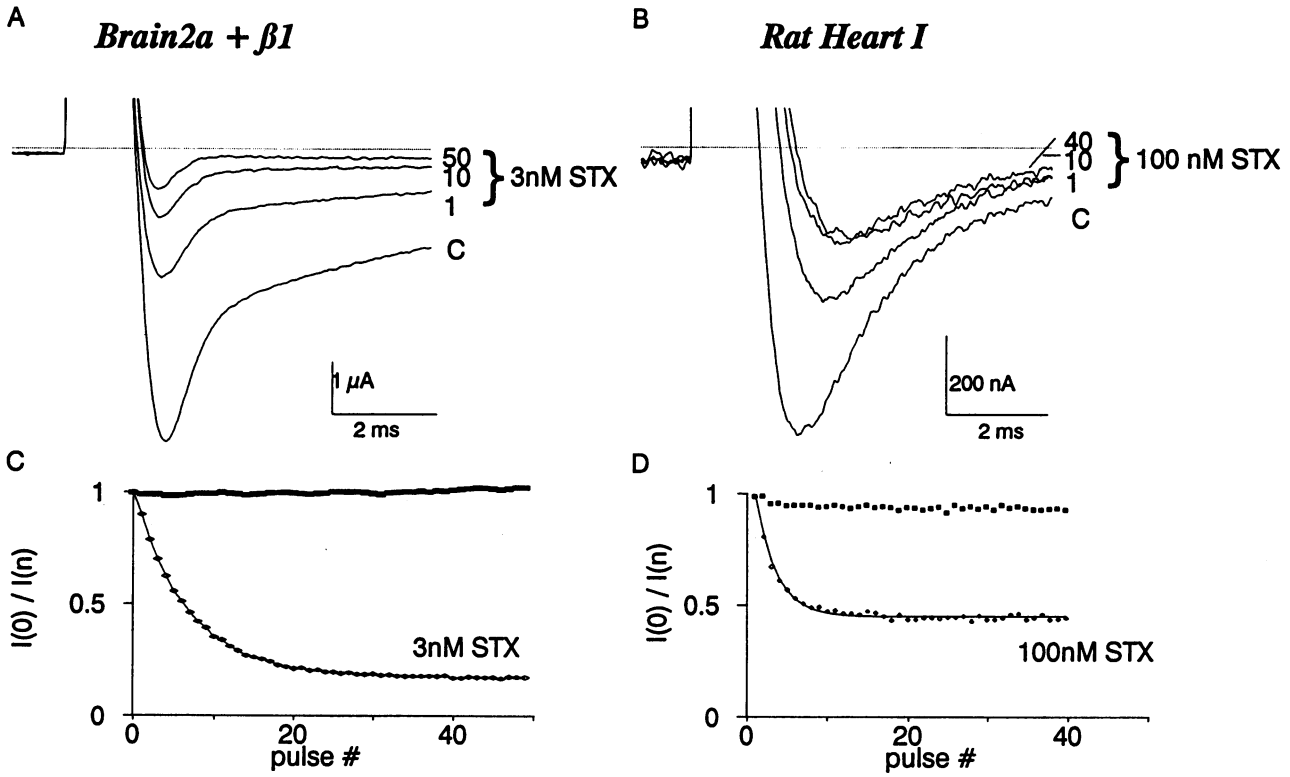

FIGURE 2 Development of phasic STX block in response to pulse trains. The rate of development of phasic block for Br2a + β1 was slower than that for RHI. Current traces for Br2a + β1 (*A*) and RHI (*B*) in the absence of STX and in the presence of an approximately half-blocking concentration of STX are shown in the top panels. The 1st, 10th, and 50th sweep (40th for RHI) in a 2 Hz pulse train of depolarizations from −100 to −10 mV for 7 ms are superimposed. Peak current amplitudes were normalized to the peak current amplitude in the initial pulse and are plotted as function of pulse number for Brain 2a + β1 (*C*) and for RHI (*D*). Peak current levels in the absence of STX (■, *C* and *D*) showed no decline during the pulse train. Peak current levels in the presence of STX (◇) are superimposed with a fit (——) to a single exponential function with τ = 9.1 pulses for Br2a + β1 and τ = 2.6 pulses for wild-type RHI. Cells e21208a and e11104c.

unblock of STX-blocked channels. The fast recovery phase is indistinguishable in the presence and absence of STX in support of the notion that this is recovery from inactivation of non-STX-bound channels. The subsequent block of channels for >100 ms after repolarization to −100 mV suggests that extra phasic block represents binding to a state that is only transiently available after recovery from inactivation. We refer to this component of toxin block that occurs after repolarization to −100 mV as post-repolarization block. Varying the conditioning potential between −10 and −30 mV had no effect on the timecourse of post-repolarization block.

The development of post-repolarization block was not recognized previously in cardiac preparations because long (>1 s) conditioning pulses were used (Cohen et al., 1981). Fig. 3 compares the effect of conditioning pulse duration on STX block. In the absence of toxin, RHI currents elicited by the two pulse protocol with a 1 s conditioning pulse recover with an additional slow phase (Fig. 3 *A*, *open squares*) compared to recovery after a 10 ms conditioning pulse (Fig. 3 *A*, *open triangles*). This additional slow phase in the absence of toxin and for the 1 s conditioning pulse is presumably recovery from slow inactivation. In the presence of 100 nM STX (about half the tonic block concentration), the rate of the fast phase of recovery is unaffected, but its normalized amplitude is diminished (Fig. 3 *B*, *filled squares*). The amplitude of phasic block after a 1 s conditioning pulse (Fig. 3, *A* and *B*, *filled squares*) is greater than that after a 10 ms conditioning step (Fig. 3, *A* and *B*, *filled triangles*); however, note that the post-repolarization block phenomenon is not apparent after the 1 s conditioning step. Apparently, relatively slow binding to a maintained state (presumably the inactivated state) during the 1 s conditioning depolarizing step obscures the post-repolarization block.

Estimation of kinetic parameters for post-repolarization phasic STX block

Fig. 4 depicts the kinetic scheme and the rate constants we used to model post-repolarization block of I_{Na} in RHI for two-pulse protocols with a 10 ms conditioning pulse. This scheme is identical to the one we used to model phasic STX block of I_{Na} in acutely isolated rat ventricular myocytes (Makielski et al., 1993a) and is a simplified four-state model for Na^+ channel gating in the absence of STX with resting (R), closed (C), open (O), and inactivated (I) states. At the resting potential, the channel is in the R state, but during a

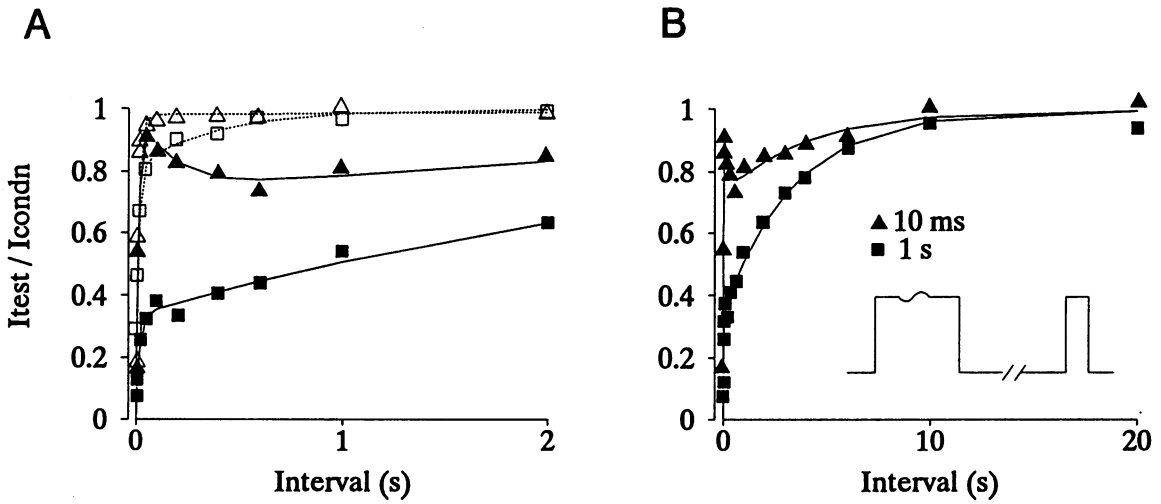

FIGURE 3 STX block of RHI current for two conditioning depolarization durations. Two types of phasic block of RHI are produced, depending upon the length of the conditioning depolarization. Peak current from a second test pulse is normalized to peak current recorded from an initial conditioning pulse that precedes the test pulse by variable intervals (see *inset* into Panel *B*). The normalized currents are then plotted against the recovery interval. Open symbols represent data in control, solid symbols represent data in 100 nM STX, triangles represent data for a 10 ms conditioning depolarization, and squares represent data for a 1 s conditioning depolarization. (*A*) Recovery data for a 10 ms conditioning depolarization in control solutions (△) were well fit (-----) by a single exponential (τ = 12 ms, a = 1). For a 1 s conditioning depolarization in control (□) a two exponential fit (·····) was required (τ_{fast} = 12 ms, a_{fast} = 0.82, τ_{slow} = 401 ms, a_{slow} = 0.18). (*B*) Results from the same experiments in 100 nM STX as in *A* are shown and include additional data to demonstrate that recovery is complete at longer intervals. For a 10 ms conditioning depolarization (▲) the data were fit to a three exponential model (——). A fast recovery phase (τ_{fast} = 13 ms, a_{fast} = 1.0), a slower development of block phase (τ_{dev} = 180 ms, a_{dev} = 0.27), and a second slow recovery phase (τ_{rec} = 3963 ms, a_{rec} = 0.27). For a 1 s conditioning depolarization (■), the data were fit to a two-exponential model (——). A fast recovery phase (τ_{fast} = 17 ms, a_{fast} = 0.35) and a slower recovery phase (τ_{slow} = 3398 ms, a_{slow} = 0.66). In all cases the rapid recovery phase was similar (τ_{fast}) and presumably represents recovery from inactivation. The development phase for a 10 ms conditioning depolarization in STX occurs *after* recovery from inactivation (post-repolarization block). Cell e20304B.

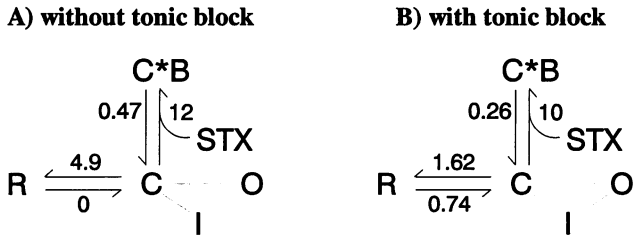

FIGURE 4 Kinetic scheme used to model post-repolarization phasic STX block for RHI. Rate constants for RHI either (*A*) not considering tonic block or (*B*) assuming tonic block occurs via binding to the same transiently available state (*C*) as phasic block. Rate constants in units of 10^6 M^{-1} s^{-1} for k_{ON}, and s^{-1} for $k_{C\to R}$, $k_{R\to C}$, and k_{OFF}. Details of the model are included in the text.

depolarizing step it rapidly transits through the C state to the O state, the process called activation; it then transits to the nonconducting inactivated state (I), the process called inactivation. After repolarization to the resting potential the channel enters the C state transiently before reaching the R state, a process called recovery. STX is postulated to bind to the C state to give the nonconducting toxin bound conformation C·B. The choice of the C state for toxin binding was dictated by the transient block shown in Figs. 3 and 5. After a 10 ms conditioning step, little or no block occurs as evidenced by the finding that for recovery intervals of 100 ms greater than 90% of I_{Na} has recovered. Therefore, STX binding to the O state and the I state were not considered further. Such an assumption would not be valid for longer conditioning steps where binding to the I state would be required to account for the block developed (Fig. 3 *A*, *filled squares*). Because binding to the R state only would account for tonic block but not for phasic block, we did not further consider binding to the R state only. To simplify the model further, we did not include the C to O, O to I, or I to C rates explicitly, but rather made the assumption that after repolarization all channels recovered to the C state rapidly relative to the STX binding rate. Thus, we assumed that all binding occurred after the repolarization step and the rate constants given are those at −100 mV.

Fig. 5 *A* shows the time course of RHI I_{Na} block for three concentrations of STX in response to a two-pulse protocol, and the solid lines represent the fit to the model with the rate constants shown in Fig. 4 *A*. For these data normalized to the conditioning pulse, the R to C transition rate was not fixed to zero but rather was a free parameter to be fit by the program. We also fit the model to data normalized to the control current to determine whether the simple model could also account for tonic block. Fig. 5 *B* shows the data normalized to control, and the solid lines represent the fit to the model with the rate constants shown in Fig. 4 *B*. This fitting shows that a nonzero R to C transition rate can account for the tonic block as well as the phasic block, without the need to postulate binding to the R state. Our data cannot discriminate

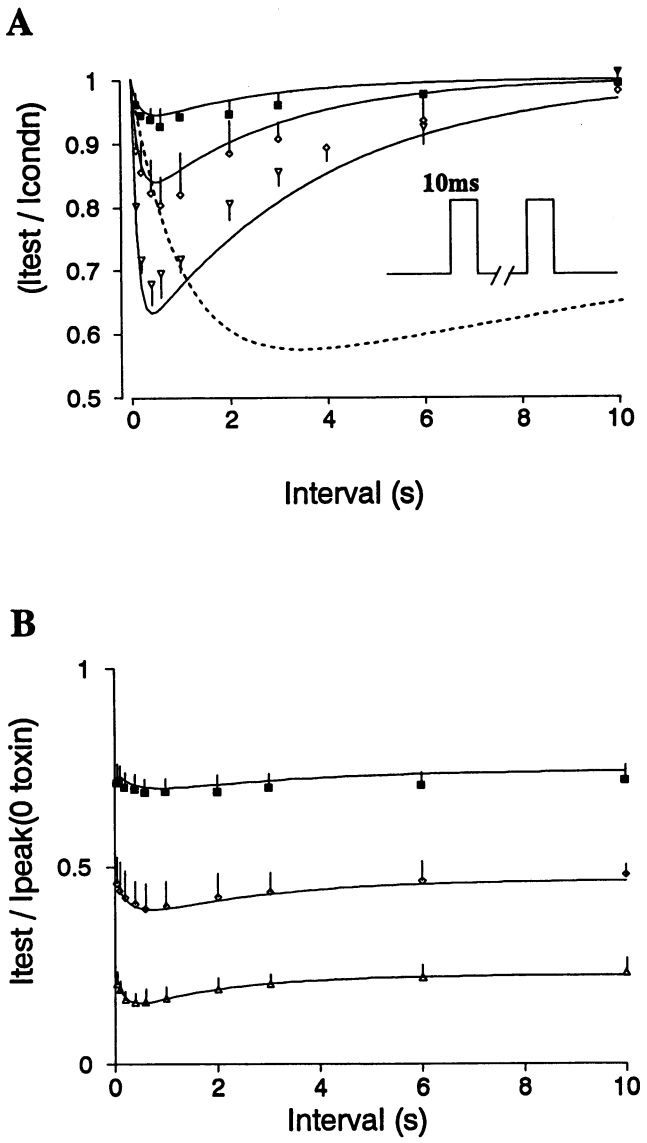

FIGURE 5 Post-repolarization phasic block by STX of I_{Na} for RHI. Normalized peak currents for three doses of STX (30 nM ■, 100 nM ◇, and 300 nM △) in response to the second (test) depolarization for a two-pulse protocol (see *inset*). From a holding potential of −100 mV a conditioning depolarizing step to −15 mV for 10 ms was followed by a variable interval at −100 mV before the test depolarization to −15 mV. Solid lines are simultaneous fits of the three doses to the model with values for rate transitions listed in Table 1 and Fig. 4. Nearly complete recovery of channels for short intervals after repolarization suggests that most channels are in a closed state from which they can open if depolarized. Development of block for longer intervals suggests that phasic block develops from a transiently available state after recovery from inactivation. (*A*) Post-repolarization phasic block for RHI without accounting for tonic block. Data represent peak current during test step (I_{test}) normalized to the peak current elicited by the conditioning step (I_{condn}). The dashed line is the fit for Br2a + β (3 nM) from Fig. 6 *A* to demonstrate the slower time course of post-repolarization block for STX-sensitive channels. (*B*) Post-repolarization phasic block with tonic block incorporated (same data as in panel *A* expressed as a fraction of the current in the absence of toxin). Current elicited by the test pulse (test) is normalized to the peak current level measured in the absence of toxin (I_{peak}, 0 toxin). (8 cells pooled, symbols ± SD).

between these models, and because we were concerned mainly with post-repolarization phasic block, we restricted further analysis to data normalized to the conditioning pulse.

Post-repolarization phasic block of Br2a + β1 has greater amplitude and slower onset and recovery than RHI (Fig. 6 *A*). Data for Br2a + β1 from Fig. 6 have also been represented as a dashed line on Fig. 5 *A* to illustrate better these differences. The same post-repolarization phasic block model for RHI was used to fit the time course of phasic block of I_{Na} for Br2a + β1 (Fig. 6; Table 1). The post-repolarization block model predicts that both a slower dissociation rate (Table 1) and longer dwell time in the transiently available non-open state (Table 1) contribute to the slower neuronal post-repolarization phasic block.

Two nonconserved residues in the putative pore-region between RHI and Br2a are critical for conferring isoform-specific tonic STX block (Satin et al., 1992a; Terlau et al., 1992). To investigate whether these pore-region amino acids affect channel kinetics as well as toxin on and off rates, we measured the kinetics of post-repolarization block of the RHI point mutants Arg^{377}→Asn and Cys^{374}→Phe. The Arg^{377}→Asn mutant is even less sensitive to STX for tonic block than RHI; Fig. 6 *B* shows the time-course of phasic block for Arg^{377}→Asn. Development and recovery from block with 100 or 300 nM STX for the Arg^{377}→Asn mutant are faster than those of the wild-type RHI (compare figs. 5 *A* and 6 *B*). Comparison of the rates derived from the three-state model shows that the dissociation rate for STX is about 5 times faster for the Arg^{377}→Asn mutant (Table 1). The model also predicted that the dwell time in the transiently available closed state is reduced for the Arg^{377}→Asn mutant (Table 1). To test for the importance of this kinetic effect, we also modeled the time-course of Arg^{377}→Asn phasic block assuming that this point mutation affected STX binding only and not channel gating (i.e., the C→R and R→C transitions). We simultaneously fit the wild-type and mutant data, forcing the R→C and C→R rates to common values for the two isoforms while allowing the STX association and dissociation rates to be fit independently. Despite the decrease in free parameters from 8 to 6, the simultaneous fit (not shown) described the data well. We conclude, therefore, that the Arg^{377}→Asn mutation does not alter dramatically the R→C and C→R transitions.

The STX-sensitive RHI mutant Cys^{374}→Phe exhibited post-repolarization block kinetics that are dramatically slower than those of RHI and were qualitatively similar to those of the STX-sensitive Br2a + β1 (compare Fig. 6, *A* and *C*), to those reported for crayfish axons (Salgado et al., 1986), and to those of frog node of Ranvier (Lönnendonker, 1989). Just as for RHI, the Cys^{374}→Phe mutant recovered rapidly (within 100 ms) from inactivation. Also, just as for RHI, post-repolarization block of the Br2a + β1 and the Cys^{374}→Phe channel occurred after recovery from fast inactivation. However, both the rate of development and the rate of recovery of phasic block are more than an order of magnitude slower for the toxin-sensitive RHI mutant Cys^{374}→Phe compared to the wild-type RHI (compare Figs.

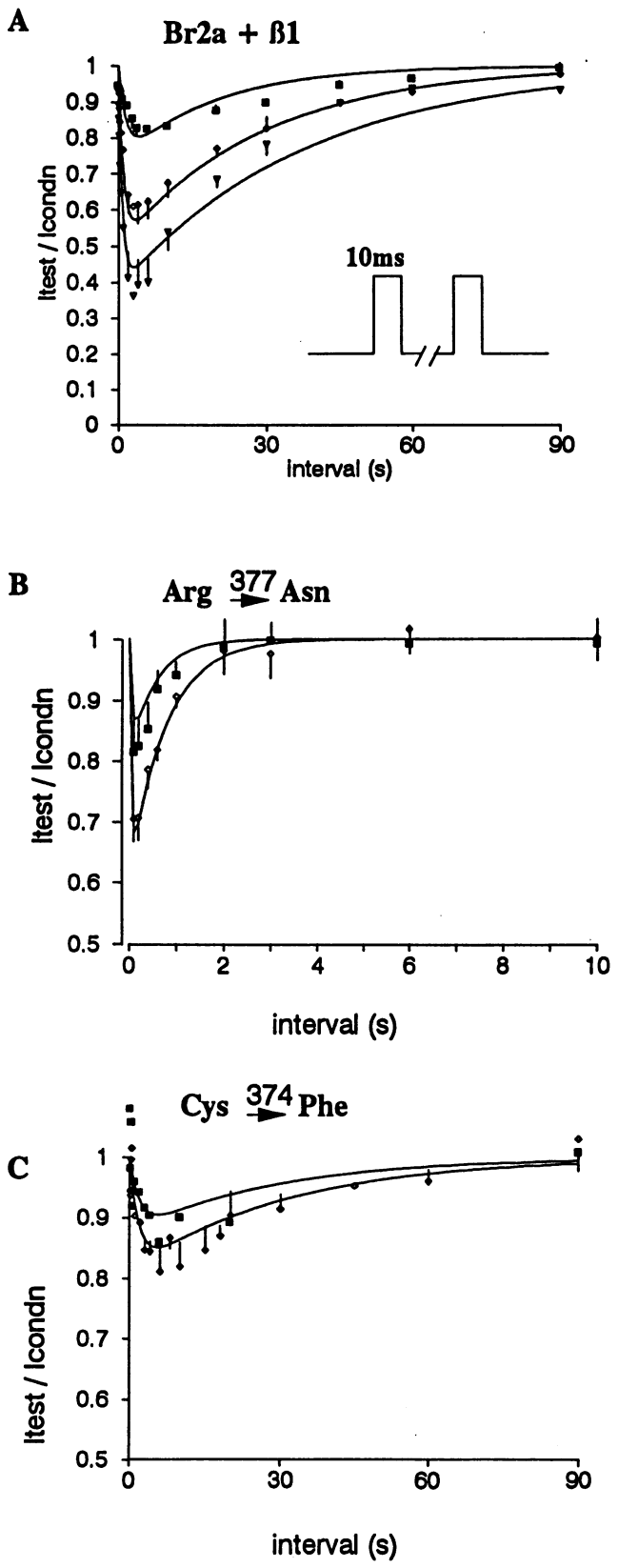

FIGURE 6 Post-repolarization phasic block of I_{Na} for STX-sensitive channels has slower kinetics than STX-resistant channels. The mean of peak currents in the second test step normalized to the peak current in the conditioning step from the indicated number of cells is shown for the two-pulse protocol (*inset* in *A*) with a 10 ms conditioning depolarization as in Fig. 5. (*A*) Data for the STX-sensitive Br2a + β1 (1.1 nM ■, 3.3 nM ◇, and 5.5 nM △ STX; n = 5 cells), (*B*) Data for the STX-resistant mutant of RHI Arg^{377}→Asn (100 nM ■ and 300 nM ◇ STX; n = 8 cells), and (*C*) Data for the STX-sensitive mutant of RHI Cys^{374}→Phe channels (3 nM ■ and 5 nM ◇ STX; n = 4 cells). The slow development of block for the STX-sensitive channels is fit by the three-state model with rates in Table 1. Note the time scale on the x axis for Br2a + β1 (panel *A*) and Cys^{374}→Phe (panel *C*) is ninefold slower than that shown for either RHI wild-type (Fig. 5 *A*) or Arg^{377}→Asn (panel *B*). The time-course of development and recovery from phasic block for both Br2a + β1, and Cys^{374}→Phe is similar to that reported for STX-sensitive channels (both native and cloned).

TABLE 1 A comparison of the STX association, dissociation rates, and the C→R transition rates among Br2a + β1, RHI, RHI mutants, and native channels calculated from the post-repolarization block model

Preparation	k_{ON}	k_{OFF}	$k_{C\to R}$
	10^6 M^{-1} s^{-1}	s^{-1}	s^{-1}
RHI	12 ± 2	0.47 ± 0.13	4.9 ± 0.8
Arg^{377}→Asn (RHI)	32 ± 0	2.26 ± 0.38	15.0 ± 3.3
Rat ventricle*	9 ± 1	0.78 ± 0.28	5.0 ± 1.1
STX-sensitive Channels			
Br2a + β1	148 ± 11	0.07 ± 0.01	0.49 ± 0.06
Cys^{374}→Phe (RHI)	20 ± 3	0.04 ± 0.02	0.44 ± 0.13

± Asymptotic SE of the parameter estimate. The R→C rate was 0 for all channel types.
* From Makielski et al., 1993.

5 *A* and 6 *C*). The maximal amplitude of post-repolarization block occurred after about 6 s in these STX-sensitive channels as compared with about 500 ms in the STX-resistant channels. The 10-fold slower C→R rate for the STX-sensitive channels (Table 1) increases the dwell time in the high affinity state C and is critical in accounting for the timing of maximal amplitude of post-repolarization block. Altering the on and off rates in this model affect only the depth of block and the rates of recovery, but do not shift substantially the timing of the maximal amplitude of post-repolarization block. The post-repolarization block for Cys^{374}→Phe has a similar time-course as for Br2a + β1, but the amplitude of the block is less than that of Br2a + β1. This difference is accounted for by a sevenfold slower association rate as determined by the model (Table 1) with no shift in the peak amplitude of block.

Post-repolarization phasic TTX block

As a test of the model and to determine whether the mechanism for TTX and STX phasic block of I_{Na} are similar, we measured post-repolarization block of wild-type RHI in the presence of TTX. For the model to be valid, fits to the block by TTX or STX should lead to identical rates for the C→R transition because in the model this step represents a conformational change of the non-toxin-bound channel. Fig. 7 shows data from a test pulse normalized to the peak current for the 10 ms conditioning pulse in the presence of 0.3, 1, and 3 μM TTX. The data for TTX block were fit to the three-state, four-rate model with the R→C rate fixed at 0 s^{-1}, and the C→R rate was fixed at 4.9 s^{-1}, the values obtained for

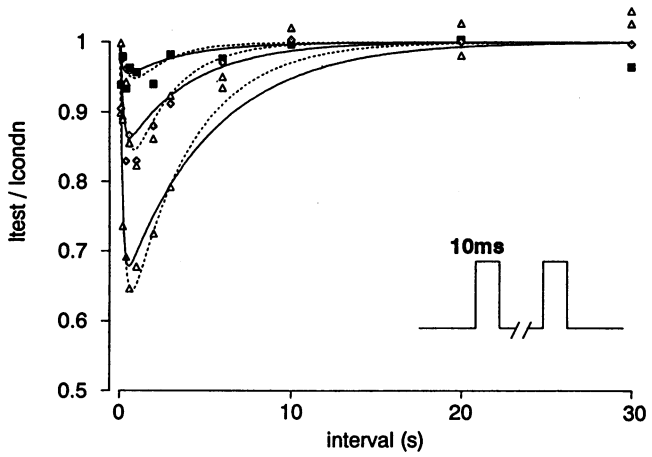

FIGURE 7 Post-repolarization block of I_{Na} for RHI by TTX. The same 2 pulse protocol as depicted in Figs. 5 and 6 was used to elicit post-repolarization phasic block. Normalized peak currents from individual experiments in 0.3 μM ■, 1.0 μM ◆ ▲, and 3.0 μM △ TTX (n = 3 cells). The lines represent fits to the three-state model. The solid lines are fits with the transition rates $k_{C\rightarrow R}$ and $k_{R\rightarrow C}$ fixed to the values obtained for RHI post-repolarization block by STX (4.9 and 0 s^{-1}, respectively, as in Fig. 5 *A*). This fit estimated the two free parameters for toxin association and dissociation to be k_{ON} = 0.92 ± 0.06 s^{-1} 10^6 M^{-1} and k_{OFF} = 0.31 ± 0.05. The dashed line is a fit with all four parameters free ($k_{C\rightarrow R}$ = 1.8 ± 0.9 s^{-1}, $k_{R\rightarrow C}$ = 0, k_{ON} = 0.6 ± 0.07 s^{-1} 10^6 M^{-1}, and k_{OFF} = 0.6 ± 0.5 s^{-1}). Increasing the number of free parameters of the fit only reduced the residual sum of squares from 0.06 to 0.04. The rates are given as the parameter estimate ± asymptotic SE of the estimate.

RHI with STX. The fit to the post-repolarization block model with only two free parameters yielded k_{ON} = 0.917 μM^{-1} s^{-1} and k_{OFF} = 0.31 s^{-1}, and the fitted lines (see Fig. 7, *solid line*) approximates the data reasonably well with a residual sum of squares of 0.06. Fitting the data allowing all four parameters to be freely fitted yielded $k_{C\rightarrow R}$ = 1.84 s^{-1}, $k_{R\rightarrow C}$ = 0, k_{ON} = 0.56 μM^{-1} s^{-1}, and k_{OFF} = 0.581 with the fitted line shown on Fig. 7 (*dashed line*) and a residual sum of squares reduced to only 0.04. We conclude that although increasing the number of free parameters from 2 to 4 did improve the fit as would be expected, the fit with 2 parameters is remarkably good and supports the use of the model for TTX with the same C→R rate as for STX.

DISCUSSION

The purpose of this study was to investigate the mechanism for isoform differences of phasic block by STX. We have shown that cloned cardiac (RHI), brain (Br2a), and pore-region RHI point mutant ($Cys^{374}\rightarrow$Phe and $Arg^{377}\rightarrow$Asn) Na channels expressed in *Xenopus* oocytes all exhibit three types of block: tonic block, phasic block in response to pulse trains, and post-repolarization block of I_{Na} by STX. Neuronal-like, high toxin affinity channels exhibit a slower development of block both in pulse trains (Fig. 2) and in two-pulse protocols (Figs. 5 and 6) than low-toxin-affinity cardiac channels. Our results suggest that the slower block kinetics in neuronal channels (compared to that of cardiac channels) can be accounted for primarily by 1) a slower toxin dissociation rate, and 2) a longer dwell time of the channel in the high affinity conformation. The RHI point mutant $Cys^{374}\rightarrow$Phe, which has similar phasic block kinetics as Br2a, also has the same dwell time in the higher affinity phasic block conformation. These results suggest that the residue at the position corresponding to amino acid 374 in RHI is essential for determining both the isoform-specific affinities for tonic block and for the conformation transition rates accounting for post-repolarization block.

Comparison with previous results and models

Phasic block is usually described in terms of the modulated receptor model (Hille, 1977) as binding to a high affinity conformation (such as the open state or the inactivated state) during the maintained depolarization. Our model represents a novel variation on this concept by placing the higher affinity state after the membrane is repolarized. Eickhorn and colleagues (Eickhorn et al., 1990) modeled phasic block of cardiac channels by TTX using guarded receptor formalism with trap and guard functions determined by the Hodgkin-Huxley model. Although accounting for inactivated state block, it cannot account for post-repolarization block, and it depends upon a particular gating model for the channel.

The Br2a + β1 and $Cys^{374}\rightarrow$Phe RHI mutant channels have post-repolarization block kinetics similar to those of the native toxin-sensitive channel in crayfish axons (Salgado et al., 1986), frog Node of Ranvier (Lönnendonker, 1989), and Br2a expressed in oocytes (Patton and Goldin, 1991). Salgado et al. (1986), who first reported the phenomenon of post-repolarization block, postulated a four-state model involving interaction with divalent ions during the interpulse interval. They did not offer any quantitative interpretation of their data in terms of this model. Lönnendonker (1989) modeled post-repolarization block as an exponentially declining toxin association rate after the membrane was repolarized. This model fit the data well, but no correlations with channel structure or gating kinetics were made. In more recent experiments Lönnendonker (1991) demonstrated that the voltage dependence of post-repolarization block followed more closely the voltage dependence of inactivation than activation. Patton and Goldin (1991) suggested from their data with Br2a channels that binding occurred to closed-state voltage-dependent transition. They postulated that the conformational change was during activation and not inactivation because a mutant channel with slowed inactivation had the same kinetics of toxin block. Consistent with the explanation of Patton and Goldin, we model block as occurring to a closed available state, but we add the refinement that block actually occurs as the channel transits this state during the recovery process. Lönnendonker's observations can be reconciled with this interpretation by assuming that the voltage-dependent distribution into the high affinity closed state occurs over a more negative voltage range (like inactivation) but does not involve inactivation itself. The fact that very

short depolarized intervals that are too brief to cause inactivation yet cause post-repolarization block (Salgado et al., 1986; Lönnendonker, 1989; Patton and Goldin, 1991) also supports this view.

Salgado et al. (1986) and Lonnendonker (1991) proposed that phasic block of toxin sensitive channels can be attributed, at least in part, to an indirect effect on the toxin association site by competition with Ca ion at a site that is further into the pore. Both toxin-resistant heart channels and toxin-sensitive brain channels show a competitive displacement of bound STX by Ca (Doyle et al., 1993). Given the structural data that the aspartic acid immediately next to Cys^{374} plays a role in Na/Ca permeability (Heinemann et al., 1992a), it is plausible that Ca affects phasic STX block. However, phasic block of RHI still occurred in the absence of external Ca (data not shown). More studies are needed to elucidate possible interactions between divalent cations, Na channel conformational changes, and block of I_{Na} by guanidinium toxins.

Differences between toxin-sensitive and toxin-resistant channels

STX and TTX binding are affected by conditions such as divalent and monovalent concentrations, temperature, and by the use of batrachotoxin in many studies. The varying experimental conditions leave some doubt as to whether the described differences are isoform-specific or attributable to study conditions. Our experiments done under identical conditions with the toxin-sensitive channels Br2a + β1 and $Cys^{374}\rightarrow$Phe show similar post-repolarization block kinetics as those reported previously for toxin-sensitive channels (Salgado et al., 1986; Lönnendonker, 1989; Patton and Goldin, 1991), and the experiments with the toxin-resistant channel RHI show the same more rapid kinetics as those reported previously for heart (Makielski et al., 1993). We conclude that the differences in phasic block kinetics are specific to the different channel isoforms.

We studied post-repolarization phasic block of the Br2a channel co-expressed with the β1 subunit to prevent accumulation of inactivated channels (Isom et al., 1992). We showed that tonic block by STX of the Br2a channel is not altered by co-expression with the β1 subunit (Fig. 1). Although we cannot exclude an effect of the β1 subunit itself on phasic block by STX, the predominant effect of the differences between toxin-resistant and toxin-sensitive channels appears to lie in the α-subunit and, in particular, in the residue occupying position 374 (RHI numbering; Cys in RH1, Phe in Br2a).

RHI wild-type compared to the STX-sensitive mutants $Cys^{374}\rightarrow$Phe display a threefold slower association rate and a 50-fold faster dissociation rate for STX. The tonic block affinity of Br2a + β1 and $Cys^{374}\rightarrow$Phe are similar. Our analysis, however, produces different on and off rates, suggesting that the binding sites are not identical. The comparison of STX versus TTX rates for the RHI wild-type also mirror the relation observed in native channels. The association rates for TTX are generally >10-fold slower than for STX, whereas the dissociation rates are similar (Guo et al., 1987).

Structural models of the Na channel (Guy and Conti, 1990; Lipkind and Fozzard, 1994) place the Cys^{374} residue in the outer pore. This region generally has not been associated with gating. Our model, however, predicts that Br2a + β1 and STX-sensitive mutant of RH1, $Cys^{374}\rightarrow$Phe, dwell longer in the higher STX-affinity conformation (C in Fig. 4) than either RHI or the less sensitive RHI mutant $Arg^{377}\rightarrow$Asn. Moreover, Br2a + β1 and the RH1 mutant $Cys^{374}\rightarrow$Phe have nearly identical fitted transition rates for C→R (Table 1). This implies that this residue in the pore-forming region affects isoform-specific conformational states of the Na channel involved in activation and recovery from inactivation. In the skeletal muscle isoform a mutation (Trp→Cys) adjacent to the homologous position to Cys^{374} in RH1 also affects kinetics (Tomaselli et al., 1993). This supports the prediction that Cys^{374} affects gating.

Limitations and predictions of the model used for phasic and post-repolarization block

The three-state model (Fig. 4) is not a comprehensive model for STX block of Na channels, but it encompasses several key features (Makielski et al., 1993) that we postulate to be a necessary part of any larger model of toxin block. These features are: 1) a cycle of a depolarization and a repolarization induces a conformational change in the channel leading to higher STX affinity; 2) this conformation exists transiently; 3) the channel must be able to open from this conformation (that is, it is not an inactivated state); and 4) a "back" reaction ($k_{C\rightarrow R}$ in this case) governs dwell time in this state and, thus, the timing of the peak block. The model was designed to account for post-repolarization and phasic block for brief (in this study 7–10 ms) depolarizing steps. As pointed out earlier (Fig. 3) STX also binds to a conformation attained during prolonged (1 s) depolarizing steps (probably an inactivated state). Our three-state post-repolarization model does not account for this maintained (inactivated) state block. Although the model can account for tonic block (Fig. 4 *B*) without requiring binding to the resting (R) state, our data cannot distinguish between models with and without binding to the R state. Simulations done with a four-state model that allowed binding to the R state (and with and without transitions allowed between the blocked state: 6 and 8 free parameters, respectively) also accounted for the data, as would be expected with more free parameters, but the key features of the model noted above remained intact.

Additional considerations concern gating of the toxin-bound state C·B. Na^+ channels bound and blocked by STX and TTX have normal gating currents (Armstrong and Bezanilla, 1974; Hanck et al., 1990), and as discussed previously for this model (Makielski et al., 1993), gating to a high affinity or "trapped" state must occur during the de-

polarizing step, because otherwise recovery from block would occur during a prolonged depolarization. The location of our putative high affinity state (C) in the context of a more complete kinetic model for channel gating, such as those proposed for heart (Scanley et al., 1990) and neuronal (Vandenberg and Bezanilla, 1991) channels, must be considered. Although we place the state adjacent to the open state (Fig. 4), this is not a necessary assumption, and it could be placed anywhere along the activation pathway. Depending upon how far the C state is from the O state, changes in time to peak, current decay, and latency might be expected when activation occurs from the putative C state (a type of Cole-Moore effect). We have modeled the transition to the high affinity conformation as coupled to the gating process, but this is not a necessary assumption. Alternatively, transition to the high toxin affinity conformation could be independent of (and parallel to) gating conformations.

CONCLUSION

A single amino acid (Cys^{374} in RH1, Phe in Br2a) affects both tonic and phasic block of I_{Na} by STX. Our analysis of the kinetics of phasic block suggests this amino acid postulated to be in the pore region also affects channel gating. Future studies to define the interactions among the gating mechanism, the permeation pathway, and the voltage sensor will contribute greatly to our understanding of structure/function relationships of voltage-gated Na channels.

We are grateful to Al Goldin for Br2a, Jim Limberis for technical assistance, and Aaron Fox for help with Axobasic 1.0.

This work was supported by a grant from the National Institutes of Health (PO1 HL20592) and Grants-in-Aid from the American Heart Association-Metropolitan Chicago (J. Satin, J. W. Kyle). Dr. Makielski is an Established Investigator of the American Heart Association.

REFERENCES

Armstrong, C. M., and F. Bezanilla. 1974. Charge movement associated with the opening and closing of the activation gates of the Na channels. *J. Gen. Physiol.* 63:533–552.

Backx, P., D. Yue, J. Lawrence, E. Marban, and G. Tomaselli. 1992. Molecular localization of an ion-binding site within the pore of mammalian sodium channels. *Science.* 257:248–251.

Baer, M., P. M. Best, and H. Reuter. 1976. Voltage-dependent action of tetrodotoxin in mammalian cardiac muscle. *Nature.* 263:344–345.

Barish, M. E. 1983. A transient calcium-dependent chloride current in the immature *Xenopus* oocyte. *J. Physiol.* 342:309–325.

Butterworth, J. F., and G. R. Strichartz. 1990. Molecular mechanisms of local anesthesia—a review. *Anesthesiol.* 72:711–734.

Carmeliet, E. 1987. Voltage-dependent block by tetrodotoxin of the sodium channel in rabbit cardiac Purkinje fibers. *Biophys. J.* 51:109–114.

Clarkson, C. W., T. Matsubara, and L. M. Hondeghem. 1988. Evidence for voltage-dependent block of cardiac sodium channels by tetrodotoxin. *J. Mol. Cell. Cardiol.* 20:1119–1131.

Cohen, C. J., B. P. Bean, T. J. Colatsky, and R. W. Tsien. 1981. Tetrodotoxin block of sodium channels in rabbit Purkinje fibers: interactions between toxin binding and channel gating. *J. Gen. Physiol.* 78:383–411.

Cribbs, L. L., J. Satin, H. A. Fozzard, and R. B. Rogart. 1990. Functional expression of the rat heart-I Na^+ channel isoform—demonstration of properties characteristic of native cardiac Na^+ channels. *FEBS. Lett.* 275: 195–200.

Delmar, M., and J. J. Jalife. 1990. Wenkebach periodicity: from deductive electrocardiographic analysis to ionic mechanisms. *In* Cardiac Electrophysiology: From Cell to Bedside, 1st Ed. D. P. Zipes and J. J. Jalife, editors. W. B. Saunders, Philadelphia, PA. 128–138.

Doyle, D. D., Y. G. Guo, S. L. Lustig, J. Satin, R. B. Rogart, and H. A. Fozzard. 1993. Divalent cation competition with ^{3}H-saxitoxin binding to tetrodotoxin-resistant and -sensitive sodium channels. A two-site structural model of ion/toxin interaction. *J. Gen. Physiol.* 101:153–182.

Eickhorn, R., J. Weirich, D. Hornung, and H. Antoni. 1990. Use dependence of sodium current inhibition by tetrodotoxin in rat cardiac muscle: influence of channel state. *Pflügers Arch.* 416:398–405.

Follmer, C. H., and J. Z. Yeh. 1988. Use-dependent block by TTX in cardiac myocytes. *Biophys. J* 53:228*a*. (Abstr.)

Guo, Z., A. Uehara, A. Ravindran, S. H. Bryant, S. Hall, and E. Moczydlowski. 1987. Kinetic basis for insensitivity to tetrodotoxin and saxitoxin in sodium channels of canine heart and denervated rat skeletal muscle. *Biochemistry.* 26:7346–7556.

Guy, H. R., and F. Conti. 1990. Pursuing the structure and function of voltage-gated channels. *TINS.* 13:201–206.

Hanck, D. A., M. F. Sheets, and H. A. Fozzard. 1990. Gating currents associated with Na channels in canine cardiac Purkinje cells. *J. Gen. Physiol.* 95:439–457.

Heinemann, S. H., H. Teriau, W. Stuhmer, K. Imoto, and S. Numa. 1992a. Calcium channel characteristics conferred on the sodium channel by single mutations. *Nature.* 356:441–443.

Heinemann, S. H., H. Terlau, and K. Imoto. 1992b. Molecular basis for pharmacological differences between brain and cardiac sodium channels. *Pflugers. Arch.* 422:90–92.

Hille, B. 1977. Local anesthetics: hydrophilic and hydrophobic pathways for the drug-receptor reaction. *J. Gen. Physiol.* 69:497–515.

Inoue, D., and A. J. Pappano. 1984. Block of avian cardiac fast sodium channels by tetrodotoxin is enhanced by repetitive depolarization but not by steady depolarization. *J. Mol. Cell. Cardiol.* 16:943–952.

Isom, L. L., K. S. Dejongh, D. E. Patton, B. F. X. Reber, J. Offord, H. Charbonneau, K. Walsh, A. L. Goldin, and W. A. Catterall. 1992. Primary structure and functional expression of the beta1- subunit of the rat brain sodium channel. *Science.* 256:839–842.

Krueger, B. K., J. F. Worley III, and R. J. French. 1983. Single sodium channels from rat brain incorporated into planar lipid bilayer membranes. *Nature.* 303:172–175.

Lipkind, G. M., and H. A. Fozzard. 1994. A structural model of the tetrodotoxin and saxitoxin binding site of the Na^+ channel. *Biophys. J.* 66:1–13.

Lönnendonker, U. 1989. Use-dependent block of sodium channels in frog myelinated nerve by tetrodotoxin and saxitoxin at negative holding potentials. *Biochimica. Biophysica. Acta.* 985:153–160.

Lönnendonker, U. 1991. Use-dependent block with tetrodotoxin and saxitoxin at frog Ranvier nodes. II. Extrinsic influence of cations. *Eur. Biophys. J.* 20:143–149.

Makielski, J. C., J. Satin, and Z. Fan. 1993. Post-repolarization block of cardiac sodium channels by saxitoxin. *Biophys. J.* 65:790–798.

Noda, M., H. Suzuki, S. Numa, and W. Stühmer. 1989. A single point mutation confers tetrodotoxin and saxitoxin insensitivity on the sodium channel-II. *FEBS. Lett.* 259:213–216.

Patton, D. E., and A. L. Goldin. 1991. A voltage-dependent gating transition induces use-dependent block by tetrodotoxin of rat IIA sodium channels expressed in Xenopus oocytes. *Neuron.* 7:637–647.

Quandt, F. N., J. Z. Yeh, and T. Narahashi. 1985. All or none block of single Na channels by tetrodotoxin. *Neurosci. Lett.* 54:77–83.

Salgado, V. L., J. Z. Yeh, and T. Narahashi. 1986. Use- and voltage-dependent block of the sodium channel by saxitoxin. *In* Tetrodotoxin, Saxitoxin and the Molecular Biology of the Sodium Channel. Vol. 479. C. Y. Kao and S. R. Levinson, editors. The New York Academy of Sciences, New York. 84–95.

Satin, J., J. W. Kyle, M. Chen, P. Bell, L. L. Cribbs, H. A. Fozzard, and R. B. Rogart. 1992a. A mutant of TTX-resistant cardiac sodium channels with TTX-sensitive properties. *Science.* 256:1202–1205.

Satin, J., J. W. Kyle, M. Chen, R. B. Rogart, and H. A. Fozzard. 1992b. The cloned cardiac sodium channel α-subunit expressed in Xenopus oocytes show gating and blocking properties of native channels. *J. Membr. Biol.* 130:11–22.

Satin, J., J. W. Kyle, R. Rogart, H. A. Fozzard, and J. Makielski. 1992c. Phasic STX block of I_{Na} is altered by point mutations of the cloned cardiac Na channel expressed in *Xenopus* oocytes. *J. Mol. Cell. Cardiol.* 24:S36*a*. (Abstr.)

Scanley, B. E., D. A. Hanck, T. Chay, and H. A. Fozzard. 1990. Kinetic analysis of single sodium channels from canine cardiac Purkinje cells. *J. Gen. Physiol.* 95:411–435.

Tomaselli, G. F., H. B. Nuss, K. Kluge, J. H. Lawrence, P. H. Backx, and E. Marban. 1993. A mutation in the pore of the Na channel alters inactivation. *Circ.* 88:987*a*. (Abstr.)

Trimmer, J. S., S. S. Cooperman, S. A. Tomiko, J. Zhou, S. M. Crean,M. B. Boyle, R. G. Kallen, Z. Sheng, R. L. Barchi, F. J. Sigworth, R. H. Goodman, W. S. Agnew, and G. Mandel. 1989. Primary structure and functional expression of a mammalian skeletal muscle sodium channel. *Neuron.* 3:33–49.

Vandenberg, C. A., and F. Bezanilla. 1991. Single-channel, macroscopic, and gating currents from sodium channels in the giant axon. *Biophys. J* 60:1499–1510.

Vassilev, P. M., R. W. Hadley, K. S. Lee, and J. R. Hume. 1986. Voltage-dependent action of tetrodotoxin in mammalian cardiac myocytes. *Am. J. Physiol.* 251:H475–H480.